Static-Pressure Probes Derived from Supersonic Slender-Body Theory

J. L. HESS* AND A. M. O. SMITH†
Douglas Aircraft Company, Long Beach, Calif.

This work describes the use of supersonic slender-body theory to derive families of noses capable of sensing static pressure substantially independent of Mach number. The theory is developed and several theoretical families of nose shapes are presented. Not only can the nose be shaped to obtain proper readings at supersonic speeds, but the afterbody too can be shaped to obtain proper readings at subsonic speeds. Both simple static probes and pitot-static probes were wind-tunnel tested at Mach numbers from about 0.1 to 5.5. Up to Mach 4 they sense static pressure well, relatively independent of Mach number. Above about 4, tests show that their readings begin to diverge from the correct values, but here the accuracy of the experiment is in doubt.

Nomenclature

A = measure of increase in cross-sectional area of afterbody [see Eq. (31)]; also coefficient in Eq. (20)
c = reference length, in particular the length of the nose of the probe
C_p = static-pressure coefficient, $(p - p_\infty)/\frac{1}{2}\rho_\infty V_\infty^2$
G = a general area distribution function [see Eq. (8)]
H = a more specialized area distribution function than G [see Eq. (12)]
M_∞ = Mach number
P = polynomials describing probe shape, Eq. (24)
q = dynamic pressure, $\frac{1}{2}\rho_\infty V_\infty^2$
R = radius of the probe
S = cross-sectional area of the probe, πR^2
t = dimensionless distance from the nose of the probe; $t = x/c$
V = velocity
x = distance, along the axis, measured from theoretical nose of the probe
β = $(1 - M_\infty^2)^{1/2}$
γ = normalized slope of the probe body at the orifice point $x = c$ [see Eq. (9)]
δ = normalized radius of the probe nose if the nose is blunt [see Eq. (7)]
ξ = a dummy variable of integration, Eq. (1)
ρ = mass density, also radius of curvature of the nose of the probe
τ = a measure of the length of transition between the nose and the final constant diameter afterbody [see Eqs. (30) and (31)]

Principal subscripts

amb = referred to conditions in the general vicinity of the probe
c = taken at the orifice point, $x = c$
inc = incompressible
n = numerical index, Eq. (20)
∞ = referred to conditions far away

Superscript

$(\ )'$ = differentiation with respect to x

1. Introduction

IN 1956 while visiting at Massachusetts Institute of Technology, the second author heard Professor E. L. Mollo-Christensen describe an ingenious static-pressure probe he had designed for supersonic wind-tunnel testing. It had a specially shaped nose such that at a particular point on it an orifice would sense static pressure independently of Mach number. This probe would not read correctly in subsonic flows, however. Now, it is well-known that the pressure at the orifice point in supersonic flow is determined entirely by the shape of the nose, that is the portion ahead of the orifice. About a year later it was realized, in view of this fact, that it is possible to modify the afterbody, that is, the portions downstream of the orifice, so that the probe could theoretically be made to read correctly for subsonic flow as well. In supersonic flow any effects of downstream shape are not perceived upstream, provided the flow is entirely supersonic and propagation of pressures through the boundary layer is negligible.

Upon recognition of the possibility of developing a probe that would be good for both sub- and supersonic Mach numbers, work was begun on the theory. Mollo-Christensen found and constructed only the most obvious nose profile.[1] The authors generalized his work, developed afterbodies, and ran wind-tunnel tests on seven different shapes, several of which had pointed, blunt, and open noses. These probes are characterized by a short nose length. On most of the models the orifices were located only 5 diam downstream of the nose. On conventional probes the orifices are usually located 10 to 15 diam to the rear of the nose. Furthermore, on most members of the family the orifices will be located ahead of the point of maximum diameter. This feature tends to give different transonic properties. On a conventional probe with orifices located well to the rear on a constant-diameter section, the shock first forms upstream and then moves across the orifices as Mach number is increased, giving a relatively severe fluctuation near $M = 1.0$. In the present type the shock tends to form behind the orifices and its effects are somewhat lessened and differ in nature.

The complete investigation of this class of probes was carried out under support of the U. S. Navy, Contracts NOw 61-0404-t, Task Order 61-4 and NOw 62-0297-t Task Order 62-7. The work is fully reported in Refs. 2–5 and 11. This work included extensive testing of the effects of pitch and yaw. Because of space limitations the present article will deal only with the case of zero angle of attack and yaw—the area in which new concepts have been developed.

2. Theory—Nose Shapes

2.1 Derivation of Restrictions on the Nose Shape from Supersonic Slender-Body Theory

Consider the probe as a slender body of revolution and let x denote axial distance measured from the tip of the probe,

Received December 27, 1966. [3.02]
* Senior Engineer/Scientist, Aerodynamics Research Group, Aircraft Division.
† Supervisor, Aerodynamics Research Group, Aircraft Division. Associate Fellow AIAA.

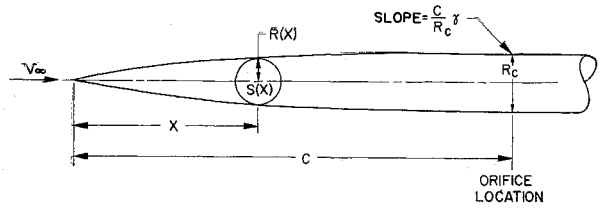

Fig. 1 Schematic diagram and notation for the probe noses.

$R(x)$ the local radius of the body contour, and $S(x) = \pi R^2$ the local cross-sectional area. The notation is illustrated in Fig. 1. The orifice location where the static-pressure probe surface is required to be equal to freestream static pressure for zero flow inclination is designated as the axial location $x = c$. It is desired to shape the probe in the region $0 \leqslant x \leqslant c$ so that the static pressure at $x = c$ equals freestream static pressure independently of Mach number. Slender-body theory is used for this purpose even though it is approximate, because it leads to simple analytic expressions and because normal probe shapes are sufficiently slender to make this theory quite accurate.

The pressure coefficient C_p at any point on the body surface is related to the shape of the probe by the well-known formula of supersonic slender-body theory (see for example Ref. 6):

$$C_p = \frac{1}{\pi} S''(x) \ln \frac{2}{R(x)(M_\infty^2 - 1)^{1/2}} + \frac{1}{\pi} \frac{d}{dx} \int_0^x S''(\xi) \ln(x - \xi) d\xi - [R'(x)]^2 \quad (1)$$

In (1) primes denote differentiation with respect to x, and M_∞ denotes freestream Mach number. It is required that $C_p = 0$ at $x = c$ for all M_∞. Observe that Mach number enters only in the first term of (1). Thus the pressure coefficient at $x = c$ is rendered independent of Mach number by requiring

$$S''(c) = 0 \quad (2)$$

A tube of constant diameter of course has this property but that is not the only possible shape.

Now, after performing the indicated differentiation in (1) and integrating by parts, the value of C_p at $x = c$, which shall be called C_{p_c}, can be written

$$C_{p_c} = \frac{1}{\pi} \int_0^c \frac{S''(x)dx}{c - x} - [R'(c)]^2 \quad (3)$$

C_{p_c} vanishes if

$$\frac{1}{\pi} \int_0^c \frac{S''(x)dx}{c - x} = [R'(c)]^2 \quad (4)$$

Equations (2) and (4) are thus the restrictions on the shape of the probe which make the static pressure at $x = c$ equal to the freestream value independently of Mach number. This is the method of Mollo-Christensen et al.[1]

There is also a restriction at the tip of the probe $x = 0$. To be a physically meaningful shape the probe must be a closed body and thus

$$R(0) = S(0) = 0 \quad (5)$$

In order to strictly satisfy the requirements of slender-body theory, the slope of the probe shape R' should be required to be finite at the tip. This would mean setting $S'(0) = 0$. For completeness it was decided to formally derive blunt probe shapes, but their validity is questionable. To exhibit explicitly the effect of nose bluntness, the shape is required to satisfy a second condition at the tip, namely

$$S'(0) = 2(S_c/c)\delta \quad (6)$$

The parameter δ is the nondimensional radius of curvature of the tip. If the actual radius of curvature of the tip is denoted ρ, then

$$\delta = (c/R_c)^2(\rho/c) \quad (7)$$

That is, δ is the ratio of tip radius of curvature to the axial distance to the orifice location, divided by the square of the thickness ratio R_c/c, where $R_c = R$ at $x = c$. If the shape is normalized by taking $R_c = c = 1$, then $\delta = \rho$.

2.2 General Equation for Probe Nose Shapes

It is convenient to express the equation for the probe nose shapes in a form where the conditions of Sec. 2.1 are identically satisfied. It now becomes convenient to write the equations in terms of the nondimensional axial distance $t = x/c$. Any function $S(x)$ that satisfies (2) can be written

$$S(t) \equiv S_c[1 + 2\gamma(t - 1) + (t - 1)^3 G(t)] \quad 0 \leqslant t \leqslant 1 \quad (8)$$

where $G(t)$ is any twice differentiable function. The constant γ is the nondimensional slope of the probe shape at $x = c$, i.e., at $t = 1$, or

$$\gamma = (c/R_c)R'(c) = [(d/dt)(R/R_c)]_{t=1} \quad (9)$$

Conversely $R'(c) = \gamma R_c/c$. The first expression in (9) shows that if $R_c = c$, γ is just the slope of the probe profile at $t = 1$. Otherwise it is the ratio of this slope to the slope of the inscribed cone with the same thickness ratio.

Applying conditions (5) and (6) to the form (8) gives

$$G(0) = 1 - 2\gamma \quad (10)$$

$$G'(0) = 3 - 4\gamma - 2\delta \quad (11)$$

The requirements may be satisfied identically by writing G in the form

$$G(t) = 1 - 2\gamma + (3 - 4\gamma - 2\delta)t - t^2 H(t) \quad (12)$$

where $H(t)$ is any twice differentiable function. The area distribution $S(t)$ thus becomes

$$S(t) = S_c\{1 + 2\gamma(t - 1) + (t - 1)^3 \times [1 - 2\gamma + (3 - 4\gamma - 2\delta)t - t^2 H(t)]\} \quad 0 \leqslant t \leqslant 1 \quad (13)$$

or, if arranged according to powers of t,

$$S(t) = S_c\{2\delta t + (6 - 6\gamma - 6\delta)t^2 - (8 - 10\gamma - 6\delta)t^3 + (3 - 4\gamma - 2\delta)t^4 + t^2(1 - t)^3 H(t)\} \quad 0 \leqslant t \leqslant 1 \quad (14)$$

Either of these forms must be differentiated twice and used in (4) to obtain the integral condition that the function $H(t)$ must satisfy. Integration by parts is used to eliminate the derivatives of H, and after considerable simplification the result is‡

$$\int_0^1 t^2 H(t)dt = \frac{1}{2}\gamma^2 - 6\gamma + 3 \quad (15)$$

Notice that this relation does not depend on δ.

‡ The theory is easily extended to the case where $C_p(c) \neq 0$. If the value of pressure coefficient at c is specified to be C_{p_c} then (15) assumes the more general form

$$\int_0^1 t^2 H(t)dt = \frac{\gamma^2}{2} - 6\gamma + 3 + \frac{1}{2}\left(\frac{c}{R_c}\right)^2 C_{p_c}$$

Later, in Sec. 4, it will be seen that slender-body theory is in error by small amounts. Designing for $C_{p_c} \neq 0$ then offers a means of correction. Except in this footnote all developments are based on the assumption that $C_{p_c} = 0$.

In summary, the pressure coefficient will vanish at $x = c$ independently of Mach number if the cross-sectional area distribution is taken in the form (13) or (14), subject to the condition (15). Expressions (13) and (14) depend on two arbitrary parameters, the nondimensional nose radius δ and the nondimensional slope γ of the shape at the orifice location, and also on an arbitrary function $H(t)$. The actual probe shape $R(t)/R_c$ is obtained by taking the square root of the term in braces in either (13) or (14), and thus either of these equations, together with (15), may be taken as the general equation of probe nose shapes.

It can thus be seen that a wide variety of nose shapes are possible corresponding to various choices of δ, γ, and $H(t)$. The thickness ratio is also available as a parameter, since $R(x)/R_c$ and $S(x)/S_c$ depend only on $t = x/c$, and thus for a given shape, an arbitrary scale change in either direction is permissible as long as the body remains slender. For purposes of discussion, probe nose shapes will generally be considered in their nondimensional form.

2.3 A Note on Shapes Having Zero Slope at the Orifice Location

For some purposes it is desired to use a probe shape having zero slope at the orifice location. For example, such a shape will have zero C_p at very high Mach numbers, according to impact theory. However, it is a very general result of the theory of the previous section that it is impossible to have a monotonically increasing probe shape with this property. That is, if a shape is calculated from (13) or (14) having $\gamma = 0$, it attains its maximum thickness at a point for which $x < c$.

To show this, assume $\gamma = 0$ and $S(x) \leqslant S_c$ for $x \leqslant c$. Then from (13)

$$1 + (t - 1)^3[1 + (3 - 2\delta)t - t^2H(t)] \leqslant 1 \tag{16}$$

so

$$t^2H(t) < 1 + (3 - 2\delta)t \tag{17}$$

and

$$\int_0^1 t^2H(t)dt \leqslant \int_0^1 [1 + (3 - 2\delta)t]dt = \frac{5}{2} - \delta \leqslant \frac{5}{2} \tag{18}$$

but (15) gives

$$\int_0^1 t^2H(t)dt = 3 \tag{19}$$

Thus if $\gamma = 0$, (15) cannot be satisfied unless $S(x) > S_c$ for some $x < c$. This property limits the usefulness of shapes having $\gamma = 0$. However, shapes can be found for which $S(x)$ exceeds S_c only slightly for $x < c$, and also shapes with very small positive values of γ can be monotonic.

2.4 Probe Nose Shapes Having Polynomial Area Distributions

A large variety of probe nose shapes can be generated by assuming the function $H(t)$ to be a polynomial. Specifically, $H(t)$ is written in the form

$$H(t) = A_0 + \sum_{n=1}^{\infty} A_n t^n \tag{20}$$

The constant term A_0 is written separately because it is this term that is found in terms of the others to satisfy the integral condition (15). Inserting (20) into (15) yields

$$\frac{1}{3}A_0 + \sum_{n=1}^{\infty} \frac{A_n}{n+3} = \frac{1}{2}\gamma^2 - 6\gamma + 3 \tag{21}$$

so

$$A_0 = 9 - 18\gamma + \frac{3}{2}\gamma^2 - 3\sum_{n=1}^{\infty} \frac{A_n}{n+3} \tag{22}$$

If this form of $H(t)$ is inserted into (13) or (14) and the terms collected, the cross-sectional area distribution can be written

$$S(t) = S_c\left[P_0 - \gamma P_\gamma + \gamma^2 P_{\gamma^2} + \delta P_\delta + \sum_{n=1}^{\infty} A_n P_n\right] \tag{23}$$

where

$$\begin{gathered} P_0 = 15t^2 - 35t^3 + 30t^4 - 9t^5 \\ P_\gamma = 24t^2 - 64t^3 + 58t^4 - 18t^5 \\ P_{\gamma^2} = \tfrac{3}{2}t^2(1 - t)^3 \qquad P_\delta = 2t(1 - t)^3 \\ 0 \leqslant t \leqslant 1 \\ P_n = t^2(1 - t)^3\left(t^n - \frac{3}{n+3}\right) \end{gathered} \tag{24}$$

Each of the P terms is a pure function of t which can be calculated once and for all. The parameters δ and γ and the combination constants A_n are independent of each other, and any of them may be taken as zero without affecting the rest. In the form (23) the cross-sectional area distribution consists of a basic function P_0 to which are added multiples of other independent modifying functions. The fact that all terms in this expression are additive makes it very convenient for calculation.

2.5 Basic Two-Parameter Family of Pointed Nose Shapes

Because blunt shapes do not satisfy the restrictions of slender-body theory, the probe shapes for $\delta = 0$ have received most of the attention. A large variety of pointed shapes were calculated from (23), and it was found that the parameter γ was far more important than any of the A_n terms in determining the general nature of the shape. Accordingly, the range of shapes determined by (23) was investigated by considering the two-parameter family involving the terms in γ and A_1 with $A_n = 0$ for $n > 1$. The "higher order" terms for $n > 1$ were reserved for effecting small changes to the shapes of the basic two-parameter family. The equation of the area distribution for this basic two-parameter family is

$$\begin{gathered} S(t)/S_c = (15 - 24\gamma + \tfrac{3}{2}\gamma^2 - \tfrac{3}{4}A_1)t^2 - \\ (35 - 64\gamma + \tfrac{9}{2}\gamma^2 - \tfrac{13}{4}A_1)t^3 + (30 - 58\gamma + \\ \tfrac{9}{2}\gamma^2 - \tfrac{21}{4}A_1)t^4 - (9 - 18\gamma + \tfrac{3}{2}\gamma^2 - \tfrac{15}{4}A_1)t^5 - A_1t^6 \\ 0 \leqslant t \leqslant 1 \end{gathered} \tag{25}$$

The one real restriction on the range of values of γ and A_1 is that the right side of (25) remain nonnegative for $0 \leqslant t \leqslant 1$. Thus in particular the coefficient of t^2 must be nonnegative. However, the range of values is also restricted, although not so precisely, by the requirement that the resulting shape be aerodynamically reasonable. The normalized shapes $R(t)/R_c$ are obtained by taking the square root of (25). Typical shapes for $\gamma = 0.1$, 0.2, 0.4, and 0.6 are shown in Figs. 2a–d, respectively, and each figure contains four values of A_1. In each figure the largest value of A_1 is the maximum that gives nonnegative cross-sectional area.

One shape of the polynomial family deserves special mention. In (25) by taking $A_1 = 0$ and $\frac{3}{2}\gamma^2 - 18\gamma + 9 = 0$, that is

$$\gamma = 6 - (30)^{1/2} = 0.52278 \tag{26}$$

the coefficients of both t^5 and t^6 vanish, and the simplest possible shape with a polynomial cross-sectional area distribution is obtained. This shape is discussed in Ref. 1.

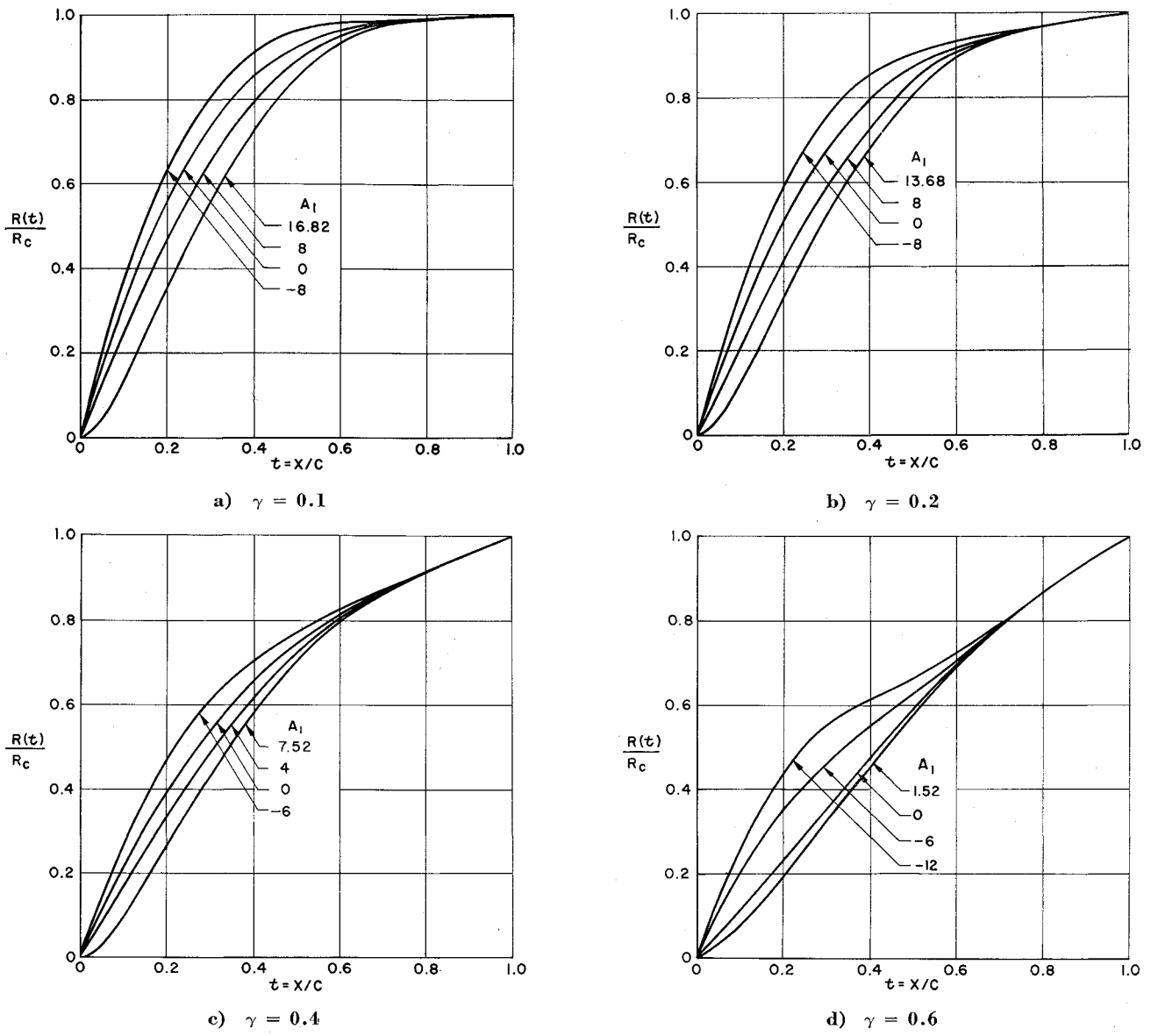

a) $\gamma = 0.1$ b) $\gamma = 0.2$

c) $\gamma = 0.4$ d) $\gamma = 0.6$

Fig. 2 Some normalized nose shapes of the basic two-parameter family.

2.6 Nose Shape Having $\gamma = 0.25$

As will be seen in Sec. 4, tests of a number of nose shapes showed that one having $\gamma = 0.25$ would develop about the minimum error in C_p. Hence a shape having $\gamma = 0.25$ with $A_1 = 4$ was studied and this is advanced as being near optimum. It has received considerable testing. The equation of this profile is

$$R(t)/R_c = (6.094t^2 - 6.281t^3 - 5.219t^4 + 10.406t^5 - 4t^6)^{1/2} \quad (27)$$

$$\gamma = 0.25 \qquad A_1 = 4 \qquad 0 \leqslant t \leqslant 1$$

3. Afterbody Shapes

3.1 General Remarks

Once the nose shape of the probe has been selected by means of the formulas of Sec. 2, the next step is to determine the probe afterbody shape, i.e., the portion of the probe downstream of the orifice location. If the probe is to serve as an isolated probe, the orifice point must read $C_p = 0$ in a freestream. For any other condition, if the probe is to measure freestream static pressure it must be remembered that in view of Bernoulli's equation, the local velocity at the orifice point c must be equal to V_∞. If the ambient region near the probe is sufficiently large to be considered a uniform stream with respect to the probe, and if the ratio $V_{\text{ambient}}/V_\infty$ is k, then the ratio V_c/V_{ambient} for the probe must be $1/k$, for

$$\frac{V_c}{V_\infty} = \frac{V_{\text{amb}}}{V_\infty} \cdot \frac{V_c}{V_{\text{amb}}} = k \cdot \frac{1}{k} = 1 \quad (28)$$

When the probe cannot be considered as an isolated body in a uniform stream large with respect to its size, then proper compensation requires solution of the entire ensemble all at once (airplane and probe) if that is possible. Conceptually, the over-all compensation problem is as illustrated in Fig. 3. The probe nose is to be at a certain position with respect to a main body, an airplane for example, whose shape of course is known. The problem is to find an afterbody shape connecting the two given bodies such that $C_{p_c} = 0$ for the combination. Obviously many afterbodies are possible. The criteria for selection are general appearance, pressure distributions, avoidance of separation, subsonic Mach number considerations, etc.

The basic determination of the afterbody is accomplished at $M_\infty = 0$, whether the interest lies in developing an isolated probe or in developing one that compensates for the presence

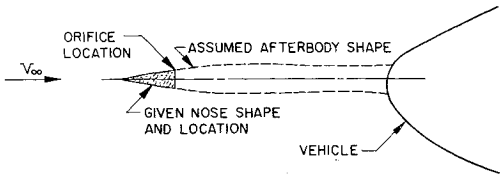

Fig. 3 Illustration of the method of determining afterbody shapes by trial and error.

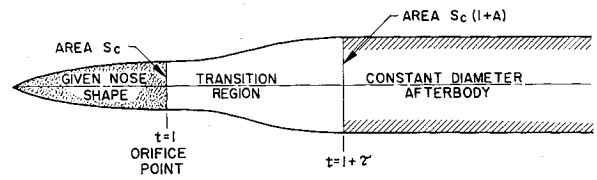

Fig. 4 Afterbody scheme using a transition region terminating as a constant-diameter boom.

of other bodies. If this compensation has been accomplished at Mach zero, the probe should sense static pressure correctly independently of Mach number for the entire subsonic range, according to subsonic slender-body theory. A well-known formula for the effect of compressibility on surface pressures on a slender body of revolution in subsonic, axially symmetric flow is[7]

$$C_p(x, R) \cong C_{p_{\text{inc}}}(x, R) - (1/\pi)S''(x) \ln\beta \qquad (29)$$

Here $C_{p_{\text{inc}}}$ denotes C_p in incompressible flow and $\beta = (1 - M_\infty^2)^{1/2}$. At the orifice point $S'' = 0$ and so again, just as in the supersonic region, Mach number dependency is removed by imposing the condition $S_c'' = 0$. Equation (29) is accurate to the order of the square of the thickness ratio.

Because the orifice location is well forward on the probe, there is no essential difference between the case when V_{ambient} is smaller than V_∞ and the case when it is larger. In the first case the afterbody curves down rather quickly and assumes its final value near the orifice location. This relatively high curvature region immediately behind the orifice location raises the velocity there relative to the local ambient stream. In the second case the afterbody increases considerably in size before it assumes its final diameter. The relatively large afterbody behind the orifice location lowers the velocity there relative to the local ambient stream. Since the particular value of V_{ambient} does not essentially alter the method of probe design, it was decided to consider the case $V_{\text{ambient}} = V_\infty$ as an example and to design afterbodies accordingly.

3.2 A Particular Afterbody

Various methods of finding the afterbody shapes are possible. One, for instance, described in Ref. 5, is to locate a number of sources along the axis and solve for their strength subject to a number of conditions. However, in view of the recent development of powerful machine computing methods[8] an indirect cut and try method will be described and illustrated by application to the $\gamma = 0.25$, $A_1 = 4$ nose shape.

It is desired to create an isolated probe having $C_{p_{\text{inc}}} = 0$ at the orifice location. To do it, the complete probe is divided into three regions: 1) the nose $0 \leqslant t \leqslant 1$, 2) a transition region $1 \leqslant t \leqslant \tau + 1$, and 3) a constant diameter final region, Fig. 4. The transition region should match S_c, S_c', and S_c'' at $t = 1$ and attain a final area $S_\tau = S_c(1 + A)$ and arrive at it with $S'(\tau + 1) = 0$. It does not seem necessary to require $S''(\tau + 1) = 0$.

The cut and try procedure is conveniently handled by devising a polynomial to describe the transition region. It contains free constants and has the end conditions properly incorporated. A suitable one is as follows:

$$S(t) = S_c\left[1 + \frac{\tau}{2}\left(\frac{t-1}{\tau}\right) + \left(4A - \frac{3}{2}\tau\right) \times \left(\frac{t-1}{\tau}\right)^3 - (3A - \tau)\left(\frac{t-1}{\tau}\right)^4\right] \qquad 1 \leqslant t \leqslant \tau + 1 \qquad (30)$$

$$S(t) = S_c(1 + A) \qquad \tau + 1 \leqslant t \qquad (31)$$

Equation (30) contains two parameters: A the fractional increase in final area over that at $t = 1$, and τ the length of the transition region, Fig. 4. The end of the transition region is at $t = \tau + 1$. By judicious and systematic variation of A and τ it is possible in a few tries to find a pair of constants (A, τ) which will make $C_{p_{\text{inc}}} = 0$ at $t = 1$. Many transition shapes are possible, short ones with small A or longer ones with larger A. Final values selected for the nose $\gamma = 0.25$, $A_1 = 4$ are

$$A = 1 \qquad \tau = 1.4 \qquad (32)$$

The primary considerations in choosing these values were appearance and mildness of surface pressure variations. Calculations of the incompressible, laminar boundary-layer flow showed that the boundary layer would not separate. Figure 5 shows a drawing of this probe as well as plots of the theoretical pressure distribution at $M = 0$, $(2)^{1/2}$, 2, and 4. Those at supersonic speed are based on the slender-body formula (1). Two nose variations that were wind-tunnel tested are also sketched. Coordinates based on (27, 30, and 31) and a table of boundary-layer corrections may be found in Ref. 5. It should not be difficult to devise a similar cut and try compensation procedure for other problems.

Table 1 Values of parameters for the probes tested

Probe II	$\gamma = 0.573$	All $A_n = 0$
Probe III	$\gamma = 0.459$	All $A_n = 0$
Probe IV	$\gamma = 0.780$	$A_1 = -3.756$ (cusped nose)
Probe V	$\gamma = 0.100$	$A_1 = 8$; $A_2 = -6.211$; $A_{10} = 12.544$
Probe VI	$\gamma = 0.800$	$A_1 = -7$; $A_2 = 20$; $A_3 = 22.18$
Probe VII	$\gamma = 0.250$	$A_1 = 4$

4. Experimental Results

Because it was realized that slender-body theory is not 100% accurate, and because no good theory was available for the transonic region, tests of several probes were made for the purpose of finding the best one. Six primary shapes were tested. Table 1 gives the values of the parameters used to obtain the nose shapes of these probes. Each probe had an afterbody designed by a method similar to that previously

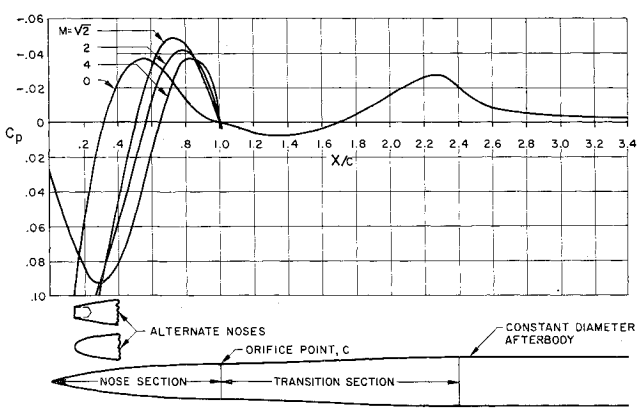

Fig. 5 Shape, alternate noses, and theoretical pressure distributions for probe VII ($\gamma = 0.25$, $A_1 = 4$).

described. Each probe was identified either by its Roman numerals or by its value of γ, which is different for each probe. A probe VIII was also tested but it was simply a more slender version of VII. Probes II–VI were selected to cover the range of γ (0.1 to 0.8) for which acceptable aerodynamic shapes can be obtained.§ These five were tested, and their results indicated a value γ of about 0.25 to be approximately best from the standpoint of errors. Accordingly, this value

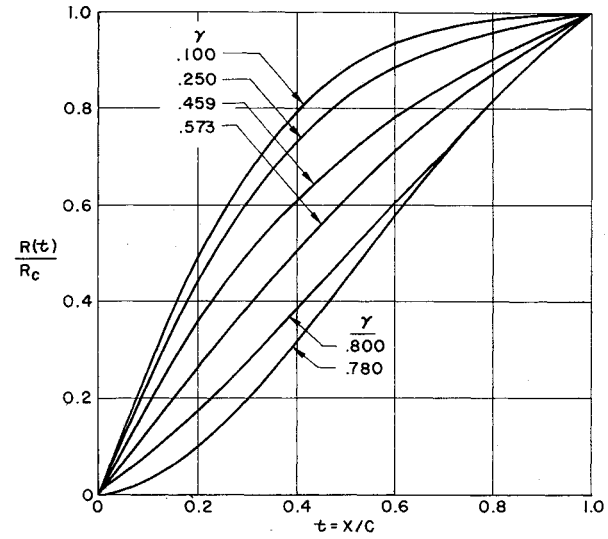

Fig. 6 Normalized nose shapes selected for testing.

was used for Probe VII. Figure 6 shows the normalized nose shapes of the probes tested.

The subsonic and transonic wind-tunnel tests were conducted in the David Taylor Model Basin 7- × 10-ft tunnel. A few check runs at low Mach number were made in the Douglas El Segundo 30- × 45-in. wind tunnel. Supersonic tests were made in the 20- × 20-in. supersonic wind tunnel at the U. S. Naval Missile Test Center, Point Mugu. All three tunnels are of continuous operation. The probes noted all had nose fineness ratios of 5, nose lengths of 3.125 in., and diameters at the point c of 0.625 in. Probes II and III were made of brass and the remainder were of stainless steel. Orifice holes at the point c were 0.0135 in. in diameter except that some checks were made with an orifice of 0.0625 in. diameter on probe VII. However, no data from this larger orifice are given in this article. All probes had a high degree of dimensional accuracy as determined on an optical comparator. The average error in diameter was about 0.0005 in. For example, on Probe VII ($\gamma = 0.25$) the maximum error in diameter over the inch centered on the orifice holes was 0.0007 in. Pressures on the orifices at point c were measured by manometers. Extra but not exceptional care was taken in these measurements, and this lack of extreme care probably accounts for some of the error and scatter to be seen later. Calibrating a basic measuring instrument is a very difficult problem, because the tunnels themselves are calibrated by other probes, and especially is this a problem in the transonic range. Much more complete details of the tests may be found in Refs. 2–4 and 11.

Figure 7 presents faired results of the supersonic tests. In these tests the lowest Mach number was 1.6 and the highest 5.5. Notice the marked influence of γ. The experimental results for probe VII ($\gamma = 0.25$) are not quite what they were predicted to be from an interpolation in γ of the results for the other probes. Because it was tested at a considerably different time, the fact that it does not exactly fit in with the rest of the family is probably due to errors of the tests.

§ Mollo-Christensen's probe was considered to be probe I.

Figure 8 is a composite plot of all the results for probe VII ($\gamma = 0.25$) obtained from tests in the continuous tunnels. Because the pointed probe is a delicate and rather lethal instrument, two alternate noses were tested, which are shown in Fig. 5. The recessed nose simulates a total head tube and the other is simply a parabolic nose that lies inside the basic $\gamma = 0.25$, $A_1 = 4$, $\delta = 0$ contour. It is not one of the δ family of blunt noses, for this contour would lie outside the pointed contour.

Probe VII was not tested in the Douglas El Segundo wind tunnel, but probe II ($\gamma = 0.573$) was. All probes were compensated sufficiently well by properly shaped afterbodies to bring $C_{p_{inc}}$ within the bounds $\pm$ 0.001. Therefore this low-speed test data should be equally applicable to probe VII.

5. Discussion

A few observations can be made about the results in Fig. 8. First of all, except for the jump at $M = 1$ the tests show that indeed the probe reads substantially independent of Mach number. The rapid change in C_{pc} at high Mach numbers is surprising; in fact it is questionable. According to Newtonian flow theory, the pressure coefficient is $C_p = 2 \sin^2\theta$ where θ is the slope of the surface. The slope of the surface of the probes at $x = c$ is so small that we can write $\sin\theta \approx \tan\theta \approx \theta$. Then in terms of our notation the pressure coefficient becomes

$$C_{pc} = 2(R_c/c)^2\gamma^2 \tag{33}$$

For probe VII, C_{pc} is computed by this formula to be only +0.00125. The highest Mach number data points clearly are not heading towards this value. Also included in Fig. 8 are calculations made by the method of characteristics. Their accuracy is unknown, but at lower Mach numbers they are in reasonable agreement with the test data, and their trend is toward the asymptotic Newtonian value. These considerations raise questions about the accuracy of the measurements at the three highest Mach numbers.

A second fact of interest is that repeat runs indicate disagreements in C_{pc} of about 0.005. This scatter confirms the findings of Ref. 9 that extreme care is necessary if errors and data scatter are really to be minimized.

A considerable search was made for data on other probes which included both the subsonic and supersonic range. The best found is that also presented in Fig. 8, obtained from Fig. 9 of Ref. 10. This probe was just a long tube of constant diameter. The data were originally in the form Δp/(impact pressure), but in Fig. 8 they have been converted to C_p. One interesting difference between the probes is in the transonic region. The NASA probe develops high positive pressures just before $M = 1$. They are probably due to a shock forming ahead of the orifices. When it moves across the orifices the pressure falls back nearly to freestream. For probe VII the opposite variation occurs. Here the shock tends to form initially downstream of the orifices,

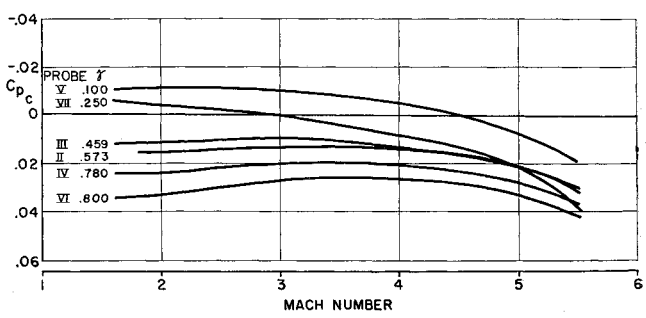

Fig. 7 Faired results of supersonic tests on the selected family of probes.

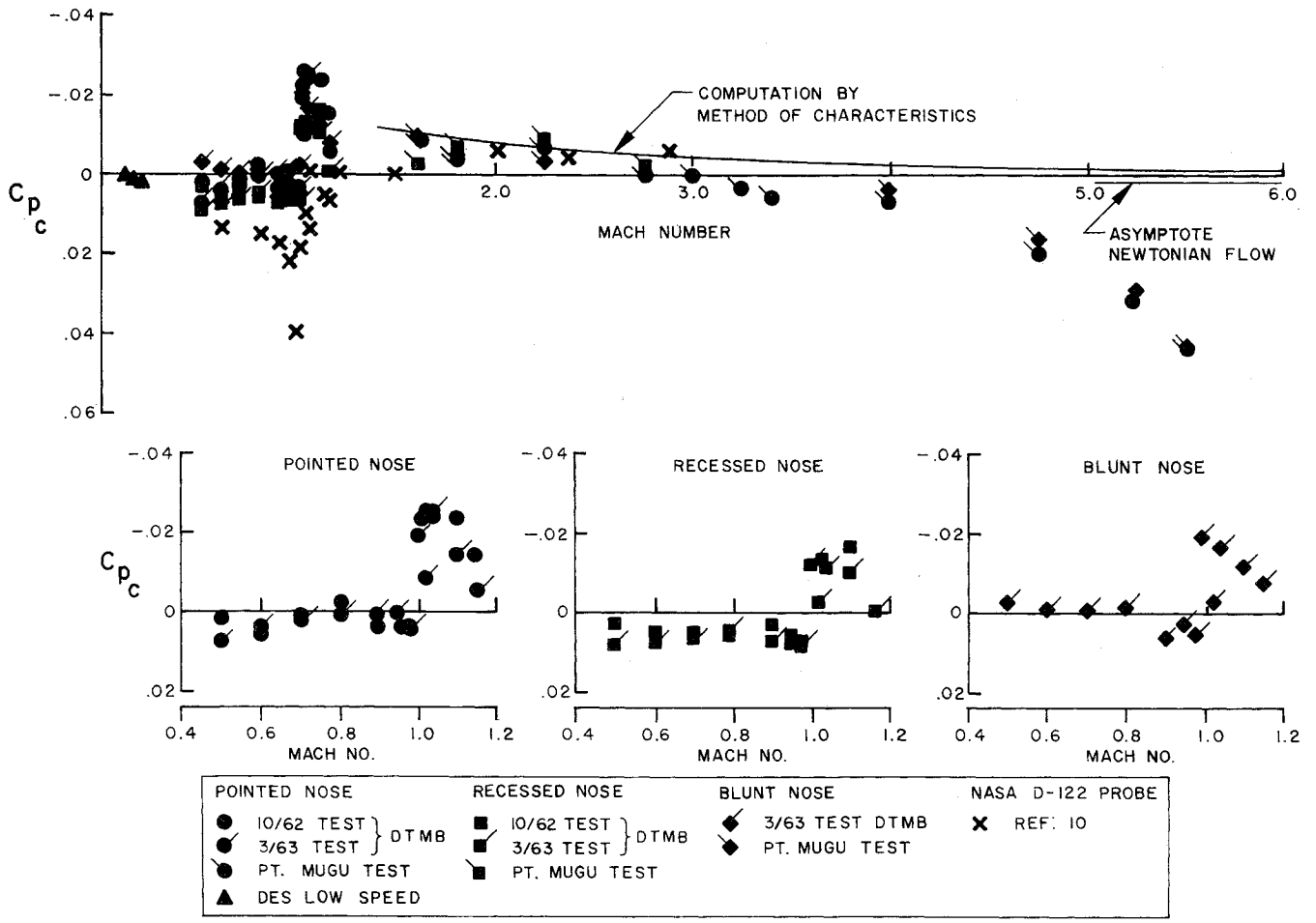

Fig. 8 Summary of test results for probe VII ($\gamma = 0.25$, $A_1 = 4$).

partially explaining the opposite sign of the transonic pressure kick.

Figure 8 includes data for the three noses sketched in Fig. 5. Generally, the recessed and blunt noses are as accurate as the pointed nose. In fact, the recessed nose has a maximum error near $M = 1$ considerably smaller than the pointed. Hence these shapes are suitable as pitot-static tubes.

A few comments should be made about nose length. On probe VII the orifices on the pointed probe are located 5 diam downstream of the nose. On the probe of Ref. 10 they are located 9 diam downstream. It is easy to apply Eq. (1) to the problem of locating orifices on a constant-diameter section downstream of a pointed nose. If the nose is parabolic and defined by

$$R(t) = R_c(2t - t^2) \qquad 0 \geqslant t \geqslant 1 \qquad (34)$$

then (1) indicates that the orifices must be located about 15 diam downstream of the nose if the theoretical error in $|C_p|$ is to be kept to 0.001 or less. In fact, the asymptotic formula for this probe is

$$C_p \sim (-R_c^2)/t^2 \qquad t \to \infty \qquad (35)$$

where R_c is the final diameter of the parabolic nose (at $t = 1$) which is then maintained. This approximate formula also indicates R_c/t must be about $\frac{1}{30}$ (15 diam) to bring C_p to about 0.001. Hence, it appears that the present probes can supply at least as good accuracy as the more conventional type for not more than about half the nose length. This feature may have advantages in certain experimental work where a longer nose may be undesirable.

References

[1] Mollo-Christensen, E. L., Landahl, M. T., and Martuccelli, J. R., "A short static-pressure probe independent of Mach number," J. Aeronaut. Sci. **24**, 625–626 (1957).

[2] Hess, J. L., Smith, A. M. O., and Rivell, T. L., "Development of improved static pressure sensing probes for all Mach numbers," Phase I, Final Report, Douglas Aircraft Co. Rept. 40336, AD 259 008L (1961).

[3] "Development of improved static pressure sensing probes for all Mach numbers," Phase II, Final Report, Douglas Aircraft Co., Contract NOw 61-0404-t Task Order 61-4, AD 466 323 (1963).

[4] "Development of improved static pressure sensing probes for all Mach numbers," Phase III, Final Report, Douglas Aircraft Co. Rept. LB 31575, AD 435 113 (1964).

[5] Hess, J. L., Smith, A. M. O., and Rivell, T. L., "Analytic design of improved static pressure sensing probes for all Mach numbers," Douglas Aircraft Co. Rept. LB 31589, AD 435 112 (1964).

[6] Liepmann, H. W. and Roshko, A., *Elements of Gas Dynamics* (John Wiley & Sons Inc., New York, 1957), p. 237.

[7] Sears, W. R. (ed.), *General Theory of High Speed Aerodynamics* (Princeton University Press, Princeton, N. J., 1954), p. 83.

[8] Hess, J. L. and Smith, A. M. O., *Progress in Aeronautical Sciences: Calculation of Potential Flow About Arbitrary Bodies* (Pergamon Press, New York, 1967), Vol. VIII.

[9] Vaugh, H. R., "A conical static pressure probe," J. Aeronaut. Sci. **28**, 829–830 (1961).

[10] Richardson, N. R. and Pearson, A. O., "Wind tunnel calibrations of a combined pitot-static tube, vane-type flow-direction transmitter, and stagnation-temperature element at Mach numbers from 0.60 to 2.87," NASA TN D-122 (1959).

[11] Kuklewicz, E. F., "Transonic wind tunnel tests of two prototype pitot-static pressure probes," David Taylor Model Basin Test Rept. AL 24 (February 1966).